ADVANCED HEALTHCARE MATERIALS
www.advhealthmat.de

Prodrug Polymeric Nanoconjugates Encapsulating Gold Nanoparticles for Enhanced X-Ray Radiation Therapy in Breast Cancer

Hamed Nosrati, Farzad Seidi, Ali Hosseinmirzaei, Navid Mousazadeh, Ali Mohammadi, Mohammadreza Ghaffarlou, Hossein Danafar, João Conde,* and Ali Sharafi**

An optimal radiosensitizer with improved tumor retention has an important effect on tumor radiation therapy. Herein, gold nanoparticles (Au NPs) and drug-containing, mPEG-conjugated CUR (mPEG-CUR), self-assembled NPs (mPEG-CUR@Au) are developed and evaluated as a drug carrier and radiosensitizer in a breast cancer mice model. As a result, cancer therapy efficacy is improved significantly by applying all-in-one NPs to achieve synchronous chemoradiotherapy, as evidenced by studies evaluating cell viability, proliferation, and ROS production. In vivo anticancer experiments show that the mPEG-CUR@Au system improves the radiation sensitivity of 4T1 mammary carcinoma and completely abrogates breast cancer.

H. Nosrati, F. Seidi
Jiangsu Co-Innovation Center of Efficient Processing and Utilization of Forest Resources and International Innovation Center for Forest Chemicals and Materials
Nanjing Forestry University
Nanjing 210037, China
E-mail: f_seidi@njfu.edu.cn

H. Nosrati, A. Hosseinmirzaei, N. Mousazadeh, A. Mohammadi, H. Danafar, A. Sharafi
Zanjan Pharmaceutical Biotechnology Research Center
Zanjan University of Medical Sciences
Zanjan, Iran
E-mail: alisharafi@zums.ac.ir

M. Ghaffarlou
Department of Chemistry
Hacettepe University
Beytepe, Ankara 06800, Turkey

J. Conde
NOVA Medical School
Faculdade de Ciências Médicas
Universidade Nova de Lisboa
Lisboa 1150-082, Portugal
E-mail: joao.conde@nms.unl.pt

J. Conde
Centre for Toxicogenomics and Human Health (ToxOmics)
Genetics
Oncology and Human Toxicology
NOVA Medical School
Faculdade de Ciências Médicas
Universidade Nova de Lisboa
Lisboa 1150-082, Portugal

The ORCID identification number(s) for the author(s) of this article can be found under https://doi.org/10.1002/adhm.202102321

DOI: 10.1002/adhm.202102321

1. Introduction

Nowadays, the most frequently developed cancer treatment modalities in clinics are radiotherapy (RT), chemotherapy, and surgery.[1] However, chemotherapeutic medicines present several drawbacks, including toxicity, adverse effects, and nonspecific dispersion.[2] The employment of nanoparticles (NPs) as biological carriers allows these challenges to be addressed and overcome some of the most challenging factors in drug delivery.

Despite the fact that radiation therapy is a common treatment for cancer,[3–5] many patients are prone to have a significant risk of cardiac toxicity, secondary malignancy, radiation pneumonitis, and lymphedema.[6–8]

Dose restriction limits the therapeutic effectiveness of RT, since radiation unavoidably damages healthy tissues surrounding the tumor.[2] Combining RT with chemotherapy improves survival and decreases tumor recurrence. Therefore, combining RT and chemotherapy is preferred for effective cancer therapy.[9,10]

Radiosensitizers are one method for preserving the therapeutic index of radiation treatment while reducing radiation-related adverse effects. In this line, NPs containing high atomic numbers (high-Z) elements have also been developed and utilized to improve RT effectiveness and specificity.[11] Under X-ray irradiation, NPs with high-Z components produce secondary and auger electrons via photoelectric and Compton processes. As a result, huge amounts of cytotoxic reactive oxygen species (ROS) are produced within the cells.[12,13] Gold nanoparticles (AuNPs), in particular, have shown to be ideal nanocarriers for radiosensitization due to their high atomic number, biocompatibility, precise size control, and adjustable surface functionalization.[14–18]

NPs have been identified as multifunctional carrier systems capable of delivering many payloads at the same time. Multifunctional NPs have been used in a variety of combination therapies. Due to its favorable chemopreventive and chemotherapeutic action, curcumin (CUR) (diferuloyl methane), a polyphenol produced from the rhizomes of turmeric, *Curcuma longa*, has gained momentum in the last years.[19–22]

Curcumin has been shown to have no toxicity to healthy organs at dosages as high as 8 g per day.[23] CUR, is also a natural-based radioprotector that can be scavenged radiation-induced free

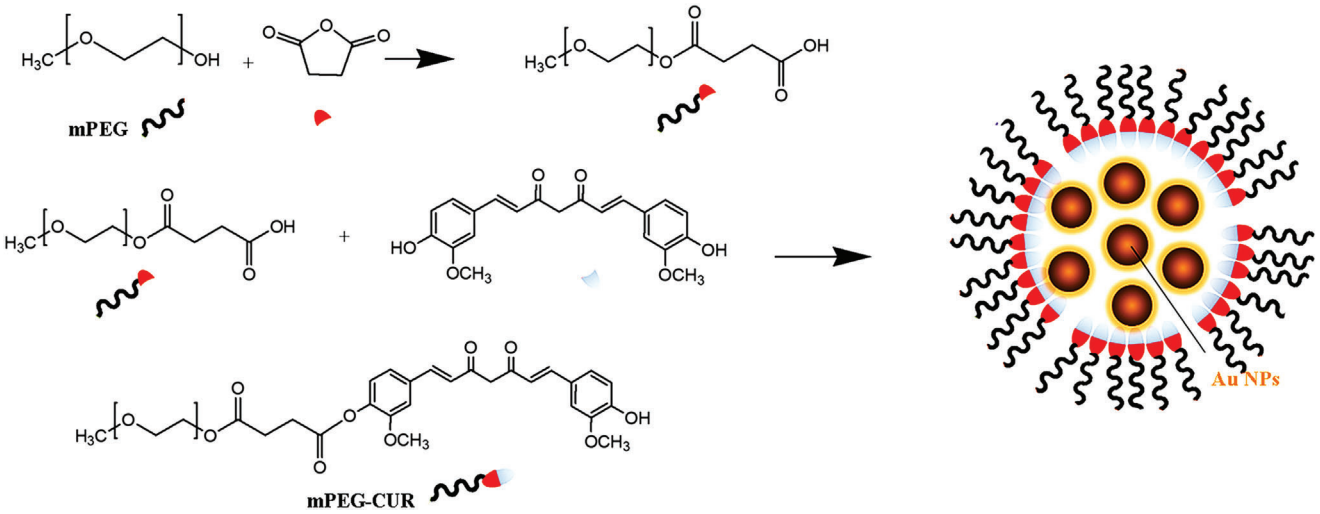

Scheme 1. Synthesis of water-soluble mPEG-conjugated CUR system (mPEG-CUR), in which CUR is covalently bonded to mPEG, to encapsulate AuNPs as radiosensitizer within polymeric mPEG-CUR NPs (mPEG-CUR@Au).

radicals, and act as a cellular antioxidant in irradiated systems.[24-26] Another method of radioprotection by curcumin might be upregulation of enzymes including catalase, glutathione transferase (GST), glutathione peroxidase (GSHpx), and superoxide dismutase (SOD) and their mRNAs. Nevertheless, CUR's effectiveness in vivo is limited by its poor solubility, low bioavailability, and poor pharmacokinetics.[27]

Herein, we developed a water-soluble mPEG-conjugated CUR system (mPEG-CUR) as an in vivo breast cancer therapy, in which CUR is covalently bonded to mPEG, to improve water solubility and targeted administration (**Scheme 1**). Moreover, we encapsulated AuNPs as a radiosensitizer within polymeric mPEG-CUR NPs (mPEG-CUR@Au) to enhance X-ray irradiation therapy efficacy. The use of a single platform with several anticancer strategy capabilities for cancer therapy saves both administration and treatment time.

2. Results and Discussion

2.1. Preparation and Characterization of the Hybrid System

Mathiyalagan et al. described a method for producing PEG conjugates.[28] The polyethylene glycol with a terminal carboxyl group (mPEG-COOH) was first prepared by reaction of mPEG with succinic anhydride and subsequently, the inserted COOH group was used for conjugation with CUR to yield the mPEG-CUR conjugate. The prepared mPEG-CUR can be self-assembled into NPs due to its amphiphilic structure. The nanoradiosensitizer (Au) was then coencapsulated in mPEG-CUR, resulting in Au-encapsulated mPEG-CUR (mPEG-CUR@Au).

The chemical structure of mPEG-CUR conjugate was characterized by HNMR technique in $CDCl_3$. The HNMR analysis of mPEG-CUR conjugate is shown in **Figure 1**a. The singlet signals at 3.2, 3.37, and 3.64 ppm represent the methoxy group of mPEG, methoxy of CUR and methylene of mPEG, respectively. The signals at 5.84 and 6.67 ppm represent the alkene double bond CH=CH of CUR. Signals at the 7.12–7.43 ppm represent the phenyl ring of CUR. This HNMR result indicates the successful conjugation of CUR and mPEG.

Furthermore, UV–Vis spectra of CUR, mPEG-CUR, and mPEG-CUR@Au are shown in Figure 1b, which confirms the presence of both CUR, and Au in the final formulation.

Regarding the UV–Vis spectrum, the characteristic Au SPR peak at 520 nm, the CUR peak at 450 nm and the mPEG-CUR@Au peak at 423 nm confirm the presence of both CUR and Au in the formulation. CUR characteristic peak in the spectrum of mPEG-CUR@Au shows a blue shift, compared to CUR spectrum, due to the interaction of CUR molecules with AuNPs in the core of NPs.

Transmission electron microscopy (TEM) images show AuNPs encapsulated by self-assembled mPEG-CUR NPs. Figure 1c,d demonstrates the formation of mPEG-CUR@Au, well-distributed and dispersed. TEM images of AuNPs show a mass of NPs, as shown Figure S1 (Supporting Information). Actually, we found that a single mPEG-CUR@Au particle contains 6-11 AuNPs (Figure 1c,d and Figure S2, Supporting Information). mPEG-CUR NPs were likewise found to have a spherical-like morphology with an average diameter of 73.8 ± 6.76 nm.

Dynamic light scattering (DLS) analysis was used to determine the hydrodynamic size of mPEG-CUR@Au in an aqueous solution. As can be seen in Figure 1e, the hydrodynamic diameter of mPEG-CUR@Au (144 ± 8 nm) was fairly bigger than the TEM image sizes, most likely due to the expansion of hydrophilic shell layers in aqueous environments.[29]

In order to evaluate stability of the NPs, we used DLS to monitor the size distribution of mPEG-CUR@Au within 30 d in deionized water and PBS. The NPs remained stable with no significant changes in size range for up to 30 days, as shown in Figure S3 (Supporting Information), showing the exceptional stability of mPEG-CUR@Au. Also, after two months of storage, there were no precipitates in the aqueous solution, which show its remarkable colloidal stability.

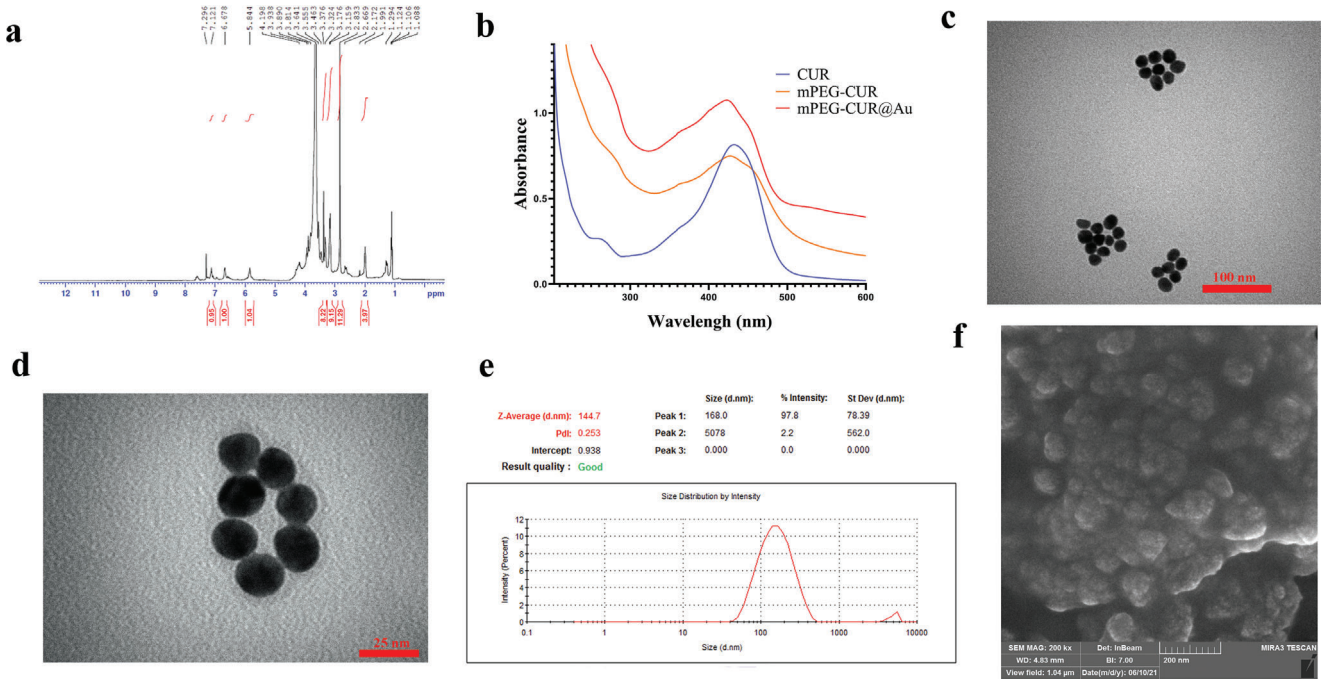

Figure 1. Characterization: a) HNMR spectrum of mPEG-CUR conjugate; b) UV–Vis spectra of CUR, mPEG-CUR, and mPEG-CUR@Au; c,d) TEM images of mPEG-CUR@Au; e) Hydrodynamic size of mPEG-CUR@Au; and f) Fe-SEM image of mPEG-CUR@Au.

In order to examine the morphology of mPEG-CUR@Au, field emission scanning electron microscopy (FE-SEM) was used to capture the microstructure image of the NPs. As shown in Figure 1f, the SEM image confirms the spherical-like morphology of mPEG-CUR@Au.

Furthermore, **Figure 2**a shows the SEM elemental EDS mapping images of the mPEG-CUR@Au in order to obtain semi-quantitative elemental results about very specific locations within the NPs surface. Elemental mappings also validate the particle structure and element distribution. The existence of C, O, and Au elements in the system was verified by EDS mapping.

The prepared AuNPs were verified to be pure Au^0 mono crystal structures by X-ray XRD.[30] Figure 2b shows the XRD pattern of AuNPs, where a number of Bragg reflections that have 2Θ values of 38.19, 44.45, 64.95, and 77.70 that correspond to the sets of lattice planes (111), (200), (220), and (311) may be indexed to the face-centered cubic (fcc) structures of AuNPs (JCPDS file no: 04-0784).[31]

2.2. Drug Loading and Releasing Studies

The loading quantity of CUR was determined to be 9.15 wt%. Under acidic conditions, the ester bond between mPEG and CUR might be cleaved, resulting in the deassembly of nanoparticles and the acceleration of drug release. Due to the breakdown of the ester bond at the acidic environment, CUR was rapidly released from mPEG-CUR@Au at pH 4.8, as shown in Figure 2c. According to the results, our prodrug nanoparticle design provided a platform for the simultaneous release of the therapeutic nanomedicines in an acidic tumor microenvironment.

2.3. In Vitro Safety Studies

2.3.1. Hemolysis Assay

The ideal formulation for an intravenous administration must be biocompatible with blood components. As a result, the hemolytic activity of the mPEG-CUR@Au at different concentrations (0, 62.5, 125, 250, 500 μg mL^{-1}) was investigated, and the red blood cells (RBC) lysis profiles were expressed as a percentage of hemoglobin released in comparison to the positive and negative controls. This is a colorimetric assay to determine the percentage of nanoparticle-induced hemolysis from the concentration of released hemoglobin when blood is exposed to nanoparticles. The findings of the hemolysis assay (**Figure 3**a) revealed that mPEG-CUR@Au have low hemolysis at all concentrations tested, suggesting that these NPs have a safe profile in vitro.

2.3.2. Toxicity Assay on Nontumorigenic Cells

Many studies have concluded that gold nanoparticles are non-toxic. By exposing nontumorigenic HEK-293 normal cells to a variety of mPEG-CUR@Au concentrations for 4 h, the capacity of mPEG-CUR@Au to cause cytotoxicity was examined. At different concentrations (0, 62.5, 125, 250, 500 μg mL^{-1}), the findings for mPEG-CUR@Au are not significantly different (Figure 3b). When HEK-293 normal cells are exposed to an mPEG-CUR@Au concentration of 500 μg mL^{-1}, only 8.5 % of them show toxicity. The colorimetric assay for assessing cell metabolic activity—MTT assay—on healthy cells also suggest that mPEG-CUR@Au is a safe candidate for both cellular and in vivo testing.

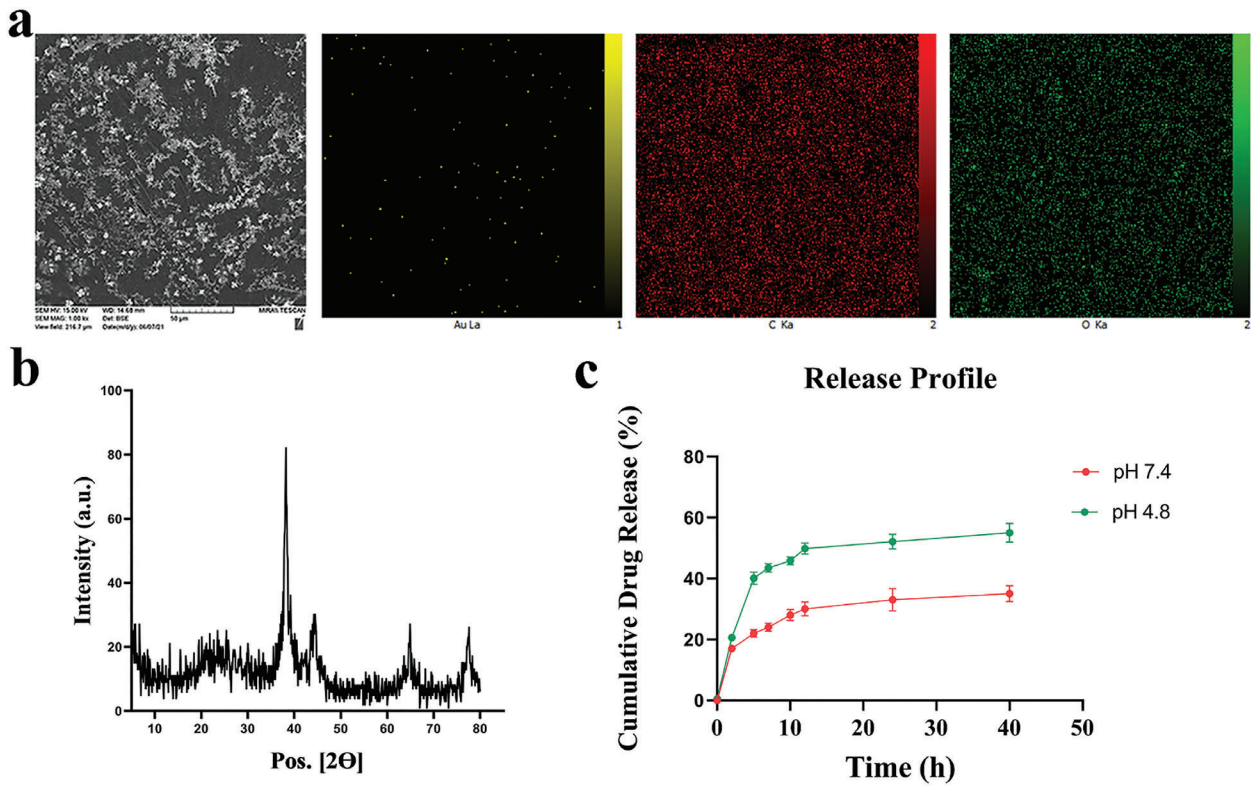

Figure 2. a) EDS elemental mapping of mPEG-CUR@Au; b) XRD pattern of mPEG-CUR@Au; and c) release profile of CUR ($n = 3$).

2.4. In Vitro Treatment Efficacy

2.4.1. Cell Viability Assay

To evaluate the toxicity effect of synthesized NPs against cancer cells, 4T1 mammary carcinoma cells were cocultured with a variety of doses of CUR, mPEG-CUR, Au, and mPEG-CUR@Au with or without X-ray irradiation.

With increasing CUR concentrations, CUR, mPEG-CUR, and mPEG-CUR@Au increased cytotoxicity against 4T1 cells was observed, as shown in Figure 3c. CUR has been shown to suppress cell growth in different cancer cells in the past.[32,33] However, compared to CUR, mPEG-CUR and mPEG-CUR@Au caused higher cytotoxicity. As demonstrated in Figure 3c, drug combinations with X-ray irradiation eliminated more cancer cells than CUR, and mPEG-CUR at each concentration. In particular, mPEG-CUR@Au, as final formulation containing CUR and AuNPs, exhibited higher inhibitory efficiency under X-ray irradiation against 4T1 cells. AuNPs induce ROS generation efficiency under X-ray irradiation.[34,37] Under X-ray irradiation, the therapeutic effectiveness of the mPEG-CUR@Au, which combined chemo and radiation treatments was higher than radiation or chemotherapy alone.

2.4.2. Colony Formation Assay

To evaluate proliferative injury in cells, the clonogenic assay with crystal violet was carried out. Clonogenic assay or colony formation assay is an in vitro cell survival assay based on the ability of a single cell to grow into a colony. As presented in the typical photographs (**Figure 4**a), cells treated with CUR + X-ray, mPEG-CUR + X-ray and mPEG-CUR@Au + X-ray showed less proliferation than those treated with X-ray and Au + X-ray, which indicated that the presence of the CUR natural drug increased the proliferative injury in cells. Moreover, groups exposed to mPEG-CUR@Au and X-rays had a low proliferation profile than mPEG-CUR and X-ray groups, which confirmed the radiosensitizing power of the AuNPs. The enhanced chemoradiation therapy efficacy was achieved not only through the radiosensitization power of the AuNPs, but also through the therapeutic power of CUR functionalized on the mPEG-CUR@Au nanoparticles, which could enhance the radiation-induced proliferative injury in cells.[34]

2.4.3. Reactive Oxygen Species (ROS) Generation Assay

Intracellular ROS generation was quantified with 2'-7'dichlorofluorescin diacetate (DCFH-DA), a cell-permeant reagent fluorogenic dye that measures hydroxyl, peroxyl, and other ROS activity in the cell. After cell uptake, DCFH-DA is deacetylated by cellular esterases to a nonfluorescent compound, which is later oxidized by ROS into 2'-7'dichlorofluorescein (DCF), producing a green fluorescence. The control group showed no green fluorescence, as illustrated in Figure 4b. However, the emitted fluorescence was higher in the irradiated group. When cells were cotreated with CUR, and mPEG-CUR and subsequently irradiated with X-rays, the intensity of the

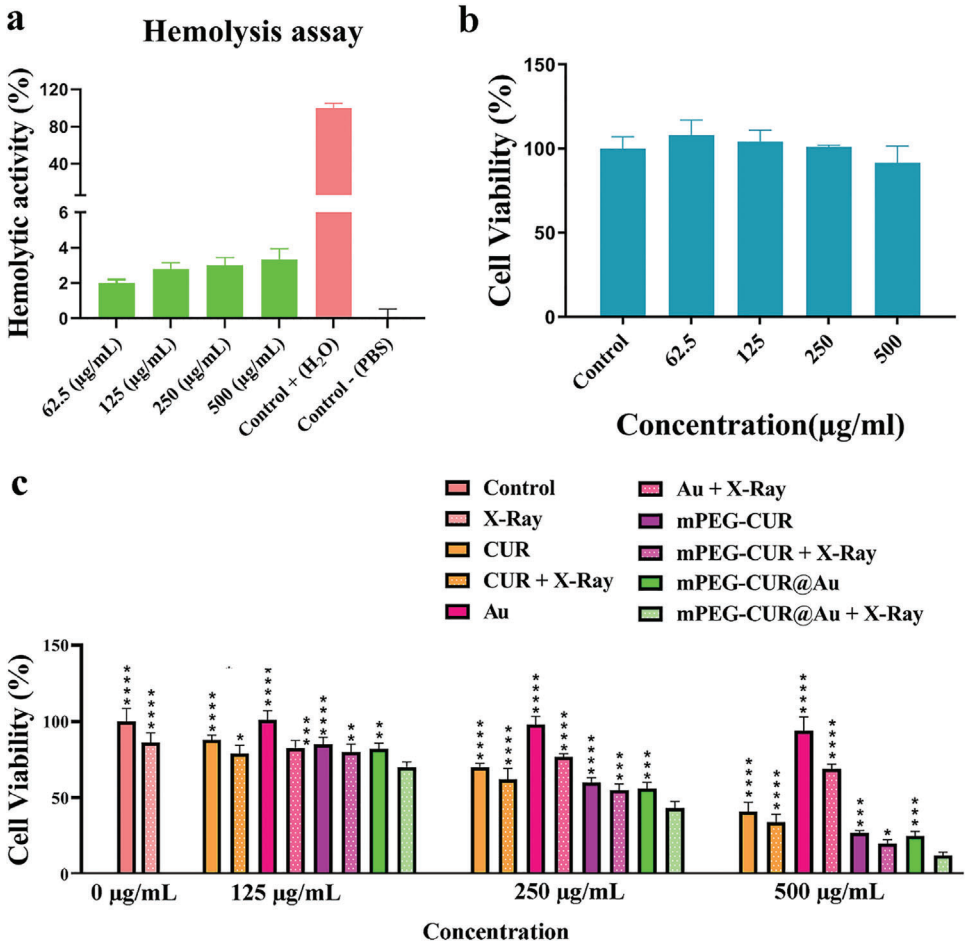

Figure 3. a) Hemolytic value of mPEG-CUR@Au at various concentration, ($n = 3$); b) Cytotoxicity assay of mPEG-CUR@Au on healthy cells ($n = 5$); c) and cell viability test on 4T1 cells incubated with different formulations in the presence and absence of X-ray irradiation (4G), ($n = 5$), (statistical test: one-way ANOVA). Data = mean ± SD; *$P < 0.05$, **$P < 0.01$, ***$P < 0.001$, and ****$P < 0.0001$ compared to the mPEG-CUR@Au + X-ray group.

fluorescence increased, which confirms the generation of ROS. When cells were treated with mPEG-CUR@Au and irradiated with X-ray, a substantial increase in fluorescence was observed. As a result, we infer that using mPEG-CUR@Au in combination with X-ray therapy might result in enhanced ROS generation, which causes more DNA damage in cancer cells.

2.5. In Vivo Treatment Efficacy

We next assessed the in vivo pharmacokinetic and therapeutic profile of the mPEG-CUR@Au NPs in an orthotopic breast cancer mouse model. Tumors in the mammary fat pad were induced in female mice by injection of 4T1 mammary carcinoma cells. mPEG-CUR@Au NPs were administered systemically via intravenous administration when tumors reached the desired volume. After intravenous injection, the biocompatibility of the synthesized NPs was evaluated. Each group consists of five mice, two of whom were euthanized three days after injection in order to further examine the anticancer impact of nanoparticles using tumor histology. Three further mice were euthanized on day 14 to allow for histopathological examination of critical organs. Data from mortality, body weight monitoring, and H&E-stained tissues revealed no significant differences compared to the control group, indicating that mPEG-CUR@Au had no negative impacts (Figure S4, Supporting Information). Additionally, no aberrant alterations were identified in H&E-stained tissues, as shown in Figure S5 (Supporting Information).

The proposed design herein of integrated multifunctional nanoplatforms combines the benefits of various therapies while compensating for the drawbacks of each monotherapy. This type of integrated nanoplatform has sparked a lot of attention since it can provide a synergistic anticancer impact.[35,36] We performed several in vivo trials to better analyze the anticancer impact of NPs after the potential effects of in vitro outcomes in synchronous chemoradiation treatment.

The relative tumor volume (V/V_0) of mice (**Figure 5**a and Figure S6, Supporting Information) revealed that when animals were treated with CUR or mPEG-CUR, and mPEG-CUR@Au without X-ray, tumor volume shows no significant changes compared to control mice. In addition, Figure 5a and Figure S6 (Supporting Information) revealed that the cotreatment of mice with CUR or mPEG-CUR and X-ray, reduced tumor development compared to control. Cotreatment with mPEG-CUR@Au

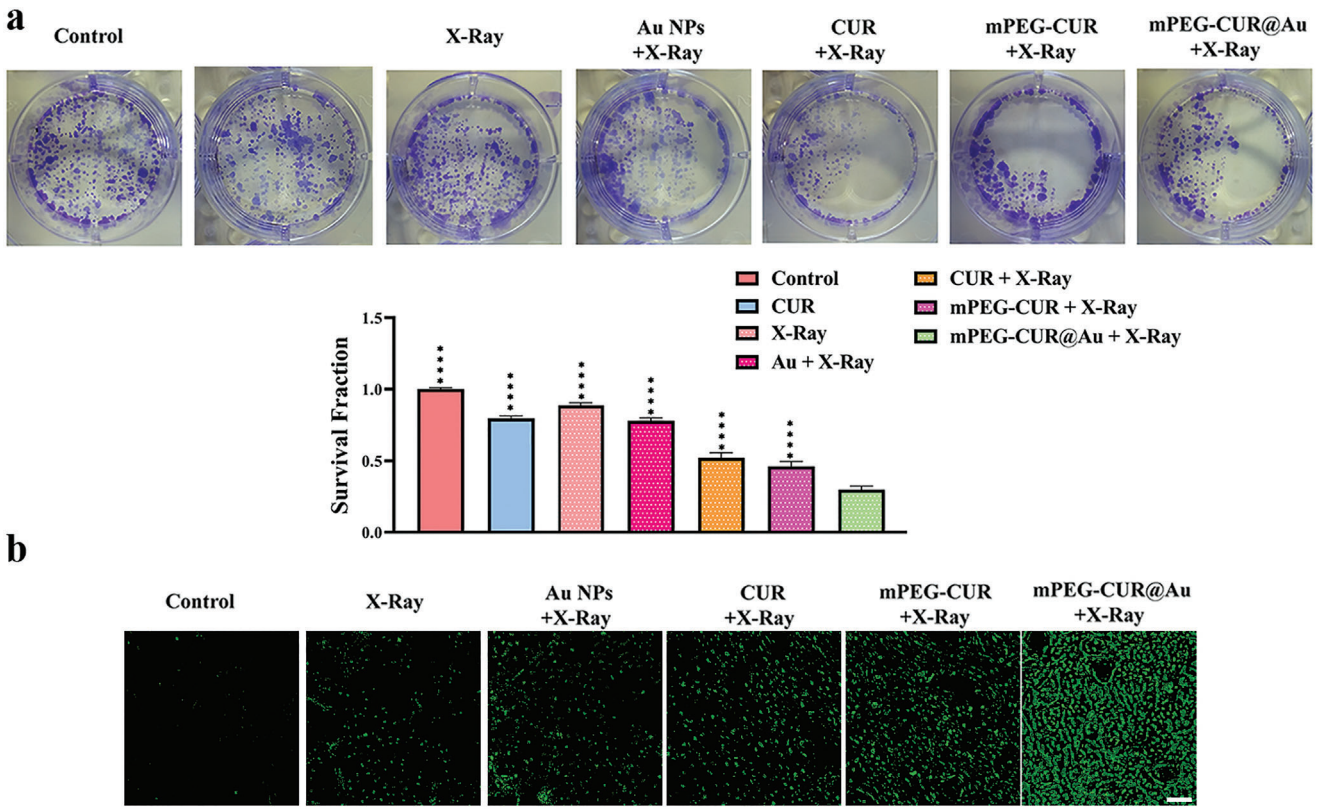

Figure 4. a) Inhibitory effects of X-rays in the presence of different formulations on the colony formation of 4T1 cells: Image and related survival fraction, (statistical test: one-way ANOVA). Data = mean ± SD; ****$P < 0.0001$ compared to the mPEG-CUR@Au + X-ray group; and b) Intracellular ROS production after various treatments in the presence and absence of X-ray irradiation. Scale bar: 40 µm.

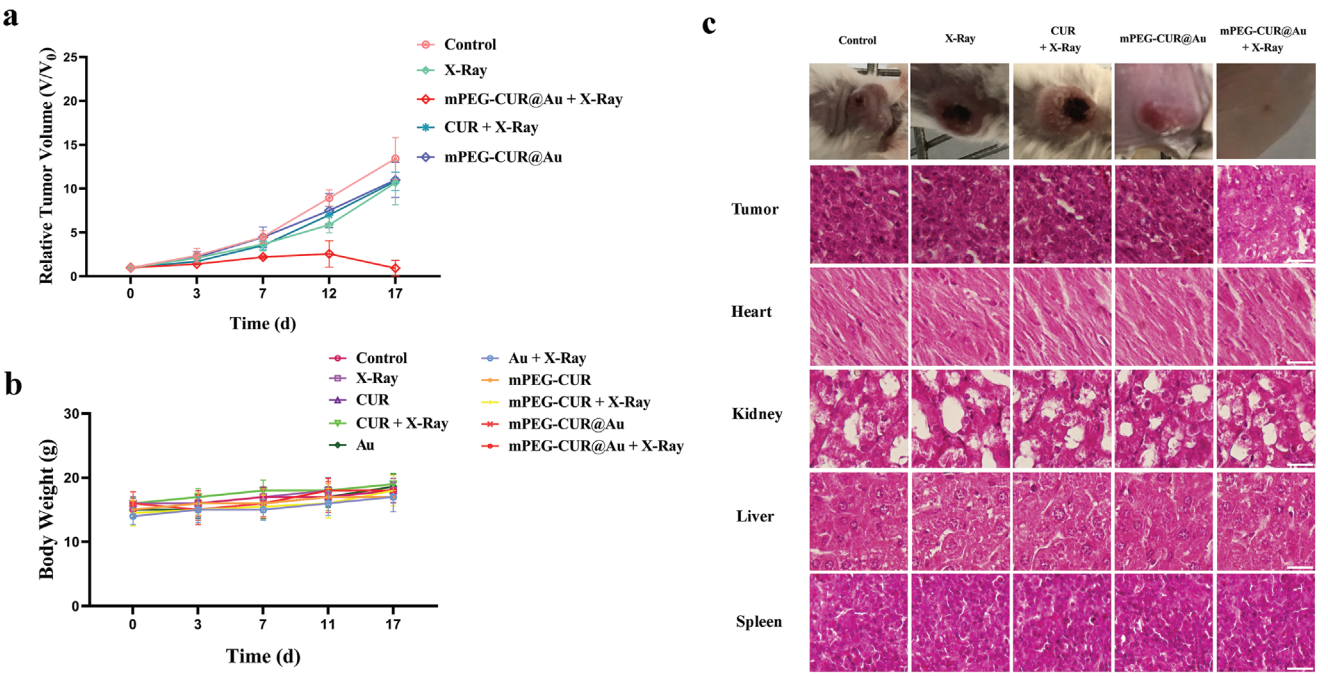

Figure 5. mPEG-CUR@Au treat breast cancer in vivo. a) Relative tumor volume, V/V_0, where V is volume of tumor in the specific day, and V_0 is the tumor volume at the beginning of treatment; b) body weight; and c) Tumor photographs and H&E-stained tumor, heart, kidney, liver, and spleen of mice treated with different treatments plans. Scale bar: 5 µm.

and X-ray reduced tumor development even more when Au was added to the system, presumably due to Au's radiosensitizing potential.[37] Finally, we discovered that simultaneous treatment with mPEG-CUR@Au combined with X-ray irradiation resulted in the tumor being eliminated in two out of five mice. Figure 5b shows that during the treatment period, no significant changes in mice's body weight were detected, indicating that nanoparticles did not cause acute toxicity in mice.

H&E staining of the tumors was done to further validate the therapeutic benefits of the different treatment strategies, as shown in Figure 5c. The densely dispersed cells in the control group have deeply stained nuclei. In the mPEG-CUR@Au + X-ray groups, necrotic and shadow regions can be seen. The experimental group, which was injected with mPEG-CUR@Au and irradiated with X-ray, was able to produce significant tumor cell death, as evidenced by a large shadow area and more necrotic-shaped cells.

Furthermore, as demonstrated in Figure 5c and Figure S7 (Supporting Information), H&E staining findings of major organs in mice with varied treatments revealed no evident tissue damage, demonstrating the nanoparticles' biocompatibility to use as in vivo therapy in breast cancer.

3. Conclusions

In conclusion, a new tumor radiosensitizer was developed based on the AuNPs containing a prodrug polymeric conjugate, made up of small gold NPs encapsulated with mPEG–CUR conjugates. Once arriving at the tumor site, the self-assembled system can collapse, and then release the drug. Also, under X-ray irradiation it can produce secondary and auger electrons, resulting in the generation of large quantities of ROS within the cells. Both in vitro and in vivo, the developed synchronous chemoradiation treatment demonstrated significant anticancer effectiveness. In a 4T1 breast cancer mouse tumor model, one-dose injection and one-time X-ray irradiation treated all five animals without recurrence. This research establishes a paradigm for converting contemporaneous chemoradiation to synchronous chemoradiation for successful cancer therapy, which might lead to new anticancer drugs and techniques being developed.

4. Experimental Section

Materials: Polyethylene glycol monomethyl ether (mPEG, M_W = 1900 Da), dimethyl aminopyridine (DMAP), trisodium citrate, and NaOH were purchased from Merck (Kenilworth, USA). Triethylamine (TEA), succinic anhydride, 1-ethyl-3-(3-dimethyl aminopropyl) carbodiimide (EDC), *N*-hydroxysuccinimide (NHS), curcumin (CUR), 3-(4,5-dimethylthiazol-2-yl)-2,5-diphenyltetrazolium bromide (MTT), 2',7'-dichlorodihydrofluorescein diacetate (DCFH-DA), crystal violet, and $HAuCl_4{\cdot}3H_2O$ were purchased from Sigma-Aldrich (St. Louis, USA). Also, chloroform, anhydrous dioxane, diethyl ether, ethanol, and acetone were purchased from Emertat Co. (Iran).

Methods: This study was approved by the Ethics Committee of the Zanjan University of Medical Sciences with the IR.ZUMS.REC.1400.98 ethical code, and the study participants signed an informed consent.

Synthesis of mPEG–COOH: Carboxyl terminus of mPEG (mPEG–COOH) was first prepared using conjugation of succinic anhydride to the hydroxyl end group of mPEG.

0.95 g mPEG (M_W 1900 g mol^{-1}; 0.5 mmol), 0.6 g succinic anhydride (0.6 mmol), 0.06 g DMAP (0.5 mmol), 20 mL anhydrous dioxane, and 0.05 g TEA (0.5 mmol) were combined for 24 h at room temperature. Cold diethyl ether was used to precipitate the resultant mPEG–COOH, which was then vacuum dried.

Synthesis of mPEG–CUR: As prepared mPEG–COOH (200 mg, 0.1 mmol), EDC (95 mg, 0.5 mmol), NHS (57.5 mg, 0.5 mmol) and NaOH were added to a round-bottom flask in 10 mL chloroform. After 10 min, CUR (44.20 mg, 0.12 mmol) was added to the stirred solution, then stirring continued for 24 h. Cold diethyl ether was used to precipitate the resultant mPEG-CUR, which was then filtered and vacuum dried.

Synthesis of Au Nanoparticles: 34 mg of $HAuCl_4{\cdot}3H_2O$ was dissolved in the 100 mL Milli-Q water at 140 °C. Next, 118 mg of trisodium citrate dihydrate in 10 mL of Milli-Q water was quickly added to the reaction mixture. After stirring for 15 min at 140 °C, the reaction solution temperature cooled to ambient temperature. Finally, excess salts were removed with the dialysis process.

Preparation of Au NPs Encapsulated within mPEG-CUR: Au NPs encapsulated within mPEG–CUR NPs by a double emulsion technique (w/o/w). Briefly, 1 mL aqueous solution of mPEG-CUR (20 mg mL^{-1}) was first poured into 2 mL acetone to form a w/o emulsion. The resulting emulsion was then injected dropwise into 20 mL of distilled water under magnetic stirring. The mixture was then magnetically stirred at room temperature to evaporation of organic solvent. This process converts the amphiphilic mPEG-CUR to self-assembled NPs. Finally, the reaction solution was centrifuged at 20 000 rpm, then the supernatant was discarded to remove unencapsulated Au NPs. As prepared mPEG-CUR@Au NPs were dispersed in Milli-Q water and stored at 4 °C.

Characterization: Characterization techniques used in this study can be found in the Supporting Information.

Drug Loading: Drug loading (DL) of mPEG-CUR@Au NPs was calculated as follow.[38] 3 mg of mPEG-CUR@Au NPs was dissolved in 1 mL ethanol. Next, UV–Vis was used to determine the quantity of Cur in the solution. Equation 1 was used to determine the DL of mPEG-CUR@Au NPs.

$$\mathrm{DL}\ (\%) = \frac{\mathrm{CUR}}{\mathrm{mPEG-CUR@Au\ NPs}} \quad (1)$$

Drug Release Study: The in vitro release behavior of CUR from NPs was investigated using a dialysis technique. mPEG-CUR@Au NPs were put in dialysis sac. The dialysis sac was drowned in 30 mL of phosphate-buffered saline (PBS, 37 °C, pH 7.4) containing ethanol (30 v/v%) and incubated with shaking (100 rpm) at 37 °C. At certain times, an aliquot was taken from the solution. The released CUR was quantified using UV–Vis.

Stability Tests: The prepared NPs stored at 4 °C in deionized water and PBS, then their stability was monitored for 30 d by DLS a different time intervals.

In Vitro Studies: Hemocompatibility: According to a previously reported protocol, the hemolytic activity assay was used to assess hemocompatibility.[38]

Cell Culture: Mouse mammary cancer cells, 4T1, and human embryonic kidney 293 cells, HEK 293 were cultured according to a previously reported protocol.[37]

Toxicity Study on Healthy Cells: Toxicity studies on HEK 293 cells were assessed by MTT assay according to a previously reported protocol.[37]

In Vitro Chemoradiotherapy: 4T1 cells were seeded in a 96-well microplates and treated at varying doses for 4 h. The cells were irradiated with X-ray (4 Gy) after being washed with PBS. There were two plates on the table. One of them was irradiated with an X-ray at a dosage of 4 Gy (6 MV), whereas the other was not.

The treated cells were then cultured for another 12 h, next the MTT test was used to determine the vitality of the cells in each well.

MTT Assay: MTT assay was done according to a previously reported protocol.[37]

Colony Formation Assay: 4T1 cells were grown in six-well plates at a density of 500 cells per well for the clonogenic test. The cells were then cultured for 48 h at 37 °C in an incubator. Following that, the cells were

given either free culture media or cell culture medium containing CUR, mPEG-CUR, Au, or mPEG-CUR@Au (mPEG-CUR@Au 250 μg mL^{-1} and an equivalent quantity of CUR and Au). The culture media in all of the wells was withdrawn after 4 h of incubation and washed with PBS before being replaced with fresh culture medium. There were two plates on the table. One of them was irradiated with an X-ray at a dosage of 4 Gy (6 MV), whereas the other was not. The cells were then cultured for another 5 d to get colony information. The culture media was thrown away and rinsed in PBS. The cells were fixed using a 3:1 mixture of methanol and acetic acid, and the fixing reagent was removed after 5 min of incubation before staining with 0.5 % crystal violet in methanol. They were then rinsed with deionized water after 15 min. Image J software was used to count the colony numbers. Finally, the cell survival fraction was calculated using the following formulas:

$$\text{Plating efficiency} = \frac{\text{Surviving colonies}}{\text{Seeded cells}} \quad (2)$$

$$\text{Surviving fraction} = \frac{\text{Surviving colonies}}{\text{Seeded cells} \times \text{plating efficiency of control}} \quad (3)$$

Reactive Oxygen Species (ROS) Generation Assay: 4T1 cells were seeded in an eight-well chamber slide and incubated for 24 h to allow for adhesion. After that, cells were cultured for 4 h with samples (CUR, mPEG-CUR, mPEG-CUR@Au, or Au) (mPEG-CUR@Au 250 μg mL^{-1} and an equivalent quantity of CUR and Au). After washing with PBS, the cells were incubated in RPMI-1640 media with 10 μM DCFH-DA for another 1 h. The cells were then exposed to X-ray (4Gy, 6 MV), seen under a fluorescent microscope, and analyzed using ImageJ software.

In Vivo Studies: Safety Study: To assess the in vivo biosafety of the mPEG-CUR@Au, it was injected at various dosages (25, 50, 100, and 200 mg kg^{-1}) into BALB/c mice ($N = 4$), then the mortality and bodyweight of them were tracked.

Furthermore, the organs' of mice treated with higher doses were stained with hematoxylin and eosin (H&E), and studied.

In Vivo Therapeutic Effect: BALB/C mice (15 g weight) were used for the evaluation of therapeutic efficacy in vivo. A total of 1×10^6 4T1 cells were subcutaneously injected into the right flank of BALB/C mice to create the 4T1 murine mammary carcinoma tumor. The mice were divided into ten groups ($N = 7$ per group) when the tumor diameters reached 60 mm^3.

100 μL of PBS, CUR, mPEG-CUR, mPEG-CUR@Au, or Au (mPEG-CUR@Au 500 μg mL^{-1} and an equivalent quantity of CUR and Au) were injected into the tail vein. 24 h after injection the tumors were either treated with X-ray irradiation at a dosage of 4 Gy (6 MV) or not. During treatment duration, the tumor volume was documented.

The following formula was used to determine the tumor volumes: tumor volume = $\text{width}^2 \times \text{length}/2$. Tumors were removed from various treatment groups on the third day after the initial injection for histological examination. After 17 d, some mice from each group were sacrificed, and their main organs were taken for histological analysis.

Statistical Analysis: All acquired data were expressed as the mean ± SD (standard deviation). Prism software was used to conduct one-way analysis of variance for various group comparisons. Significant differences between the groups were indicated by * ($P < 0.05$), ** ($P < 0.01$), *** ($P < 0.001$), or **** ($P < 0.0001$).

Ethical Considerations: This study was approved by the Ethics Committee of the Zanjan University of Medical Sciences with the IR.ZUMS.REC.1400.98 ethical code, and the study participants signed an informed consent.

Supporting Information

Supporting Information is available from the Wiley Online Library or from the author.

Acknowledgements

This work was supported by the Deputy of Research of Zanjan University of Medical Sciences (A-12-848-30). J.C. acknowledges financial support from the European Research Council – ERC Starting Grant 848325.

Conflict of Interest

J.C. is a co-founder and shareholder of TargTex S.A.

Data Availability Statement

Research data are not shared.

Keywords

chemoradiation therapy, drug conjugates, gold nanoparticles, high-Z nanoparticles, radiosensitizers

Received: October 26, 2021
Published online: December 2, 2021

[1] Y. Chen, G. Song, Z. Dong, X. Yi, Y. Chao, C. Liang, K. Yang, L. Cheng, Z. Liu, *Small* **2017**, *13*, 1602869.
[2] Y. Chang, L. He, Z. Li, L. Zeng, Z. Song, P. Li, L. Chan, Y. You, X.-F. Yu, P. K. Chu, *ACS Nano* **2017**, *11*, 4848.
[3] B. Fisher, J. Costantino, C. Redmond, E. Fisher, R. Margolese, N. Dimitrov, N. Wolmark, D. L. Wickerham, M. Deutsch, L. Ore, *N. Engl. J. Med.* **1993**, *328*, 1581.
[4] L. Portelance, K. C. Chao, P. W. Grigsby, H. Bennet, D. Low, *Int. J. Radiat. Oncol. Biol. Phys.* **2001**, *51*, 261.
[5] S. S. Jeppesen, T. Schytte, H. R. Jensen, C. Brink, O. Hansen, *Acta Oncol.* **2013**, *52*, 1552.
[6] S. C. Darby, M. Ewertz, P. McGale, A. M. Bennet, U. Blom-Goldman, D. Brønnum, C. Correa, D. Cutter, G. Gagliardi, B. Gigante, *N. Engl. J. Med.* **2013**, *368*, 987.
[7] K. Henson, P. McGale, C. Taylor, S. Darby, *Br. J. Cancer* **2013**, *108*, 179.
[8] T. DiSipio, S. Rye, B. Newman, S. Hayes, *Lancet Oncol.* **2013**, *14*, 500.
[9] A. Choudhury, R. Swindell, J. P. Logue, P. A. Elliott, J. E. Livsey, M. Wise, P. Symonds, J. P. Wylie, V. Ramani, V. Sangar, *J. Clin. Oncol.* **2011**, *29*, 733.
[10] T. Mitin, D. Hunt, W. U. Shipley, D. S. Kaufman, R. Uzzo, C.-L. Wu, M. K. Buyyounouski, H. Sandler, A. L. Zietman, *Lancet Oncol.* **2013**, *14*, 863.
[11] Y. Zang, L. Gong, L. Mei, Z. Gu, Q. Wang, *ACS Appl. Mater. Interfaces* **2019**, *11*, 18942.
[12] Q. Liu, Y. Shi, Y. Chong, C. Ge, *ACS Appl. Bio Mater.* **2021**, *4*, 1843.
[13] W. Fu, X. Zhang, L. Mei, R. Zhou, W. Yin, Q. Wang, Z. Gu, Y. Zhao, *ACS Nano* **2020**, *14*, 10001.
[14] J. F. Hainfeld, F. A. Dilmanian, D. N. Slatkin, H. M. Smilowitz, *J. Pharm. Pharmacol.* **2008**, *60*, 977.
[15] S. Jain, D. Hirst, J. O'sullivan, *Br. J. Radiol.* **2012**, *85*, 101.
[16] X.-D. Zhang, D. Wu, X. Shen, J. Chen, Y.-M. Sun, P.-X. Liu, X.-J. Liang, *Biomaterials* **2012**, *33*, 6408.
[17] A. Al Zaki, D. Joh, Z. Cheng, A. L. B. De Barros, G. Kao, J. Dorsey, A. Tsourkas, *ACS Nano* **2014**, *8*, 104.
[18] Y.-S. Yang, R. P. Carney, F. Stellacci, D. J. Irvine, *ACS Nano* **2014**, *8*, 8992.

[19] B. K. Jaggi, S. C. Chauhan, M. Jaggi, *Proc. S. D. Acad. Sci.* **2007**, *86*, 283.
[20] S. Karmakar, N. L. Banik, S. J. Patel, S. K. Ray, *Neurosci. Lett.* **2006**, *407*, 53.
[21] S. Shishodia, H. M. Amin, R. Lai, B. B. Aggarwal, *Biochem. Pharmacol.* **2005**, *70*, 700.
[22] S. Shishodia, M. M. Chaturvedi, B. B. Aggarwal, *Curr. Probl. Cancer* **2007**, *31*, 243.
[23] C. Hsieh, *Anticancer Res.* **2001**, *21*, e2900.
[24] B. Farhood, A. Aliasgharzadeh, P. Amini, H. Saffar, E. Motevaseli, S. Rezapoor, F. Nouruzi, D. Shabeeb, A. E. Musa, G. Ashabi, *Medicina* **2019**, *55*, 317.
[25] H. Bagheri, S. Rezapour, M. Najafi, E. Motevaseli, B. Shekarchi, M. Cheki, H. Mozdarani, *Iran. J. Med. Sci.* **2018**, *43*, 645.
[26] M. Ahmed, M. A. Qadir, A. Hameed, M. N. Arshad, A. M. Asiri, M. Muddassar, *Bioorg. Chem.* **2018**, *76*, 218.
[27] G. Garcea, D. Jones, R. Singh, A. Dennison, P. Farmer, R. Sharma, W. Steward, A. Gescher, D. Berry, *Br. J. Cancer* **2004**, *90*, 1011.
[28] R. Mathiyalagan, Y. J. Kim, C. Wang, Y. Jin, S. Subramaniyam, P. Singh, D. Wang, D. C. Yang, *Artif. Cells, Nanomed., Biotechnol.* **2016**, *44*, 1803.
[29] K. H. Bae, M. Park, M. J. Do, N. Lee, J. H. Ryu, G. W. Kim, C. Kim, T. G. Park, T. Hyeon, *ACS Nano* **2012**, *6*, 5266.
[30] Q. Yu, J. Li, Y. Zhang, Y. Wang, L. Liu, M. Li, *Sci. Rep.* **2016**, *6*, 1.
[31] H. Nosrati, Y. Baghdadchi, R. Abbasi, M. Barsbay, M. Ghaffarlou, F. Abhari, A. Mohammadi, T. Kavetskyy, S. Bochani, H. Rezaeejam, *J. Mater. Chem. B* **2021**, *9*, 4510.
[32] M. Kumari, N. Sharma, R. Manchanda, N. Gupta, A. Syed, A. H. Bahkali, S. Nimesh, *Sci. Rep.* **2021**, *11*, 1.
[33] A. J. Van Der Vlies, M. Morisaki, H. I. Neng, E. M. Hansen, U. Hasegawa, *Bioconjugate Chem.* **2019**, *30*, 861.
[34] N. Yu, Z. Wang, J. Zhang, Z. Liu, B. Zhu, J. Yu, M. Zhu, C. Peng, Z. Chen, *Biomaterials* **2018**, *161*, 279.
[35] T. S. Hauck, T. L. Jennings, T. Yatsenko, J. C. Kumaradas, W. C. Chan, *Adv. Mater.* **2008**, *20*, 3832.
[36] J. Qiu, Q. Xiao, X. Zheng, L. Zhang, H. Xing, D. Ni, Y. Liu, S. Zhang, Q. Ren, Y. Hua, *Nano Res.* **2015**, *8*, 3580.
[37] H. Nosrati, E. Attari, F. Abhari, M. Barsbay, M. Ghaffarlou, N. Mousazadeh, R. Vaezi, T. Kavetskyy, H. Rezaeejam, T. J. Webster, *Bioact. Mater.* **2022**, *7*, 74.
[38] H. Tang, C. J. Murphy, B. Zhang, Y. Shen, E. A. Van Kirk, W. J. Murdoch, M. Radosz, *Biomaterials* **2010**, *31*, 7139.